Thermal Updraft Profiling with an Array of Show Drones

Pedro Lacerda[1,2,3], Gábor Vásárhelyi[1,2] and Máté Nagy[1,3,4*]

Abstract— **Localized thermal convective updrafts in the atmosphere, commonly referred to as thermals, serve as a significant source of energy-efficient flight for birds, human pilots, and autonomous aircraft. Measuring the vertical airspeed distribution within these updrafts to estimate their strength and characteristics is a significant empirical challenge. In this study, we introduce a proof-of-concept distributed thermal measurement system that uses small, cost-effective multirotor drones equipped with standard sensors, eliminating the need for specialized airspeed instruments. These drones estimate updraft strength by analyzing performance parameters such as power consumption or rotor rotation speed. First, we conducted extensive investigations in a simulated environment that incorporated varying windy conditions to establish the relationship between the updraft speed (the vertical speed of the air) and the performance parameters of the drones. Following this, we conducted outdoor experiments involving up to 49 multirotor drones to demonstrate the effectiveness of the distributed measurement system in action. By advancing our understanding of thermal updrafts, this research contributes valuable information to analyze avian flight behavior and also facilitates the development of realistic simulation environments. These advancements can enhance the design of thermal-utilizing self-driving algorithms for unmanned aerial vehicles (UAVs), paving the way for more efficient and adaptive robotic systems.**

I. INTRODUCTION

WHEN the sun heats the ground, the ground warms the layer of air directly above it, creating a Rayleigh-Bénard instability [1]. These systems often result in coherent structures known as thermal plumes (or simply thermals), i.e. localized columns of rising air encompassed by a downdraft caused by the displacement of colder air. Within the thermal, air rises to thousands of meters above the ground. This process is responsible for the formation of cumulus clouds and has a significant impact on the transport of energy and humidity in the mixed layer of the atmosphere [2].

The measurement of thermal updraft phenomena could be of relevance for fundamental meteorological sciences, by better understanding atmospheric convection and its consequences on Global Circulation Models [3]. On a local scale, thermals are also frequently used as a free source of energy by many bird species on their long migrations [4] and foraging activities [5]–[7] as well as by humans for leisure activity using aircrafts such as gliders, paragliders

[1]Department of Biological Physics, Eötvös University, Budapest, Hungary

[2]CollMot Robotics Ltd., Budapest, Hungary

[3]MTA-ELTE ‘Lendület’ Collective Behaviour Research Group, Hungarian Academy of Sciences, Budapest, Hungary

[4]Department of Collective Behaviour, Max Planck Institute of Animal Behavior, Konstanz, Germany

*corresponding author: nagymate@hal.elte.hu

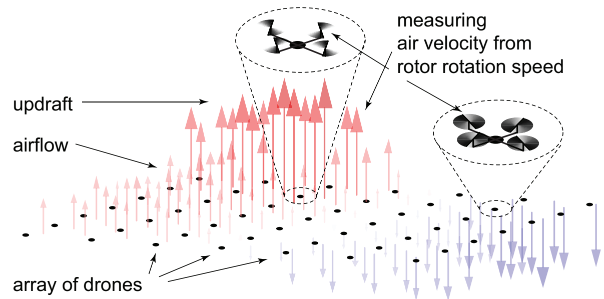

Fig. 1. **Overview of the concept of the experimental setup.** A fleet of multirotor drones is used as a distributed sensor array to estimate the motion of the air from the rotor rotation speeds.

or hanggliders [8]. In the same manner, autonomous flying vehicles (mostly gliders but also other UAVs) could benefit from understanding and using these updrafts for a potential increase of their energy efficiency [9], [10]. The thermal air velocity field estimated from distributed measurements could be used to create an internal thermal model for training AI-driven vehicles and advancing previous research on thermalling gliders [11]–[16].

As a large-scale phenomenon, atmospheric convective updrafts are impossible to measure in a laboratory setting, while in-situ measurements are very challenging and consequently very scarce and have been performed only with limited resolution in time or space [17]–[20]. However, in the past decade, a new possibility arose for measuring the atmosphere due to the emergence of very capable commercial drones at low prices.

Multirotors (hereafter referred to as *drones*), in particular, have proven to be a very flexible and cost-effective solution for probing our atmosphere for meteorological measurements [21], [22], in particular for horizontal wind estimation [23]–[26]. Measurements of vertical movements of the air are much scarcer: to our knowledge, there is one work in which fixed-wing drones were used [27], and one experiment that used a multirotor drone [28].

Within the diverse emerging portfolio of drones, we are particularly interested in show mini-drones used for aerial displays for the following reasons: i) they have reached very small physical size and weight due to legal, logistics and safety requirements and thus their interference with the air mass is as low as possible; ii) they possess professional-grade, RTK-based, cm-level positioning capabilities due to commercial show quality requirements; iii) they are available at relatively low price and in large quantities, and can be inherently controlled easily as a swarm with proper software, available even open-source [29].

Here we propose a method for an indirect measurement of the air velocity field within thermals using a fleet of such show mini-drones as a distributed sensing array, without the need to carry specialized measuring equipment onboard (Fig. 1). Looking for characteristic flight performance indicators such as power consumption or rotor rotation speed upon encountering different updrafts, we achieve distributed, spatiotemporal sampling of air velocities.

To achieve this, first, we conducted Software-In-The-Loop (SITL) simulations to work out the measurement methodology and to investigate the relation between directly measured flight parameters and indirectly estimated vertical wind velocity. Simulations also serve as a means for validating the concept before real experiments and showcase how our method works under controlled and known conditions. As a next step, we follow our custom-designed calibration protocol using real drones in open air to investigate the performance and quantify the possible reality gap between simulations and field experiments. Finally, we perform distributed measurements with a relatively large drone fleet.

II. METHODS

The proposed procedure for estimating airspeed consists of two phases. First, each drone needs to be calibrated (preferably in still air) to find the exact functional form between the directly measured performance parameter, such as the rotor rotation speed, and the indirectly estimated airspeed. Then in the second phase, the calibrated drone can be utilized to estimate the velocity of the air by hovering at a given location. Additionally, we can perform measurements with previously uncalibrated drones by combining the two phases, and perform the calibration and the measurement with post-processing.

A. Calibration protocol

The calibration protocol uses a predefined spatio-temporal trajectory where the drone moves upwards and downwards with a set of desired speeds for predefined time intervals, with a period of hovering in between to stabilize. This procedure was repeated with increasing desired speeds to map the entire range of vertical velocity relative to the air. The desired horizontal velocities were kept at $0 ms^{-1}$ at all times to avoid drifting sideways by the wind. We studied this protocol both in simulation and in field experiments.

B. Simulation

1) Simulation Runs: A software-in-the-loop (SITL) approach was utilized to study this system in a simulation. Microsoft AirSim [30] was used as the base flight simulator environment engine. Simulated drones with a dedicated fork of the ArduCopter 4.4 SITL firmware [31] were controlled using a multi-UAV control framework, Skybrush [29] (developed by CollMot Robotics Ltd).

Each drone moved along a predefined trajectory with the protocol explained above, where the magnitude of the desired vertical velocity for the upward and downward motion ranged from 0.5 to 3.5 ms^{-1} in increments of 0.5 ms^{-1}.

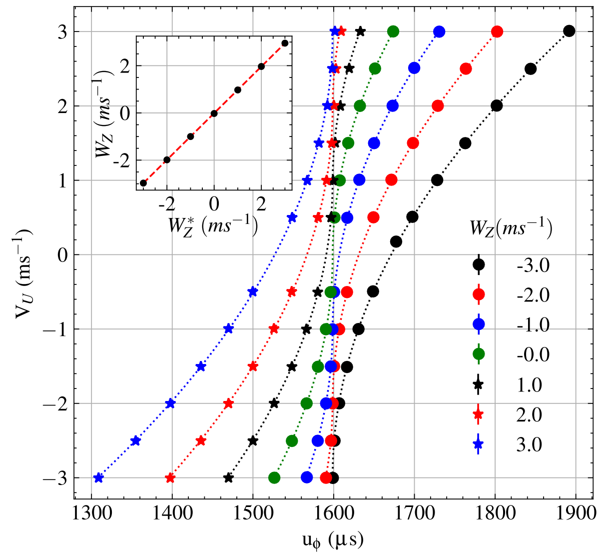

Fig. 2. **Performance of the drones in the simulations and corresponding fitted curves in windless conditions with different updraft strength.** Markers correspond to the mapping between local averages of the pulse width of the speed controller (u_ϕ) as a proxy for rotor thrust and local averages of the actual vertical velocity (V_{U}), in the presence of different updrafts indicated by the color. The dotted lines are the corresponding best fit for each simulation, where the color of the line match that of the markers. The inset on the top left corner shows the match between the estimated updraft (W_{Z}^*, horizontal axis) and the actual updraft (W_{Z}, vertical axis) resulting from the simulation. The red dashed line indicates $W_{\mathrm{Z}} = W_{\mathrm{Z}}^*$.

The constant-speed sections were kept for 20 seconds, with 10 seconds of hovering between consecutive vertical motion phases. This protocol was repeated for (horizontal) wind magnitude of 0 ms^{-1}, 2.5 ms^{-1} and 5 ms^{-1} in 6 different directions. The vertical velocity of the air (modeled as a homogeneously distributed vertical wind to mimic different down- and updrafts) was also varied, ranging from -3.5 ms^{-1} to 3.5 ms^{-1}. These settings were set in the AirSim framework as environmental parameters.

The low-level flight controller of the drone (ArduCopter) logged the required status information about the flight, which was analyzed offline after the simulated experiments.

2) Analysis: The resulting flight logs were split into time intervals (windows), i.e., periods of constant desired velocity. At the beginning of each window, there is a transient phase of acceleration, where the actual velocity may significantly differ from the final target velocity. Based on the flight logs, we conservatively assumed that the drone stabilized its velocity within 10 seconds. Therefore, for each 20-second window, only the last 10 seconds were used for the analysis. Furthermore, to accommodate for errors in the alignment of the time windows, the last second of each window was also omitted.

Using these windows, median and standard deviation statistics were calculated for the actual vertical velocity (V_{U}), the Rotor Control Pulse Width (RCPW) signal of the flight controller (u), which is proportional to the rotation speed of the rotor, roll angle (ν), pitch angle (θ) and power. Since we are only interested in the vertical component of

TABLE I

RESULT OF THE FITTED PARAMETERS FOR THE SIMULATION USING (4)

$A \quad (10^{-6}m^{-2}s^{3})$	8.207 ± 0.020
$u_{\phi,0} \quad (\mu s)$	1598.656 ± 0.039
$W_Z^* \quad (ms^{-1})$	-0.0589 ± 0.0031

TABLE II

FITTING PARAMETERS AND THEIR STATISTICS, INCLUDING THE REDUCED-χ^2 (χ^2_ν) FOR EACH FITTING FUNCTION.

Function	parameter	average ± s.d.	χ^2_ν
signed quadratic	A $(10^{-6}\ m^{-2}s^{3})$	10.5 ± 2.6	2.19 ± 0.84
	$u_{\phi,0}$ (μs)	1562 ± 42	
	W_{Z} (ms^{-1})	0.4 ± 3.0	
linear	A' $(10^{-6}\ m^{-1}s^{2})$	26.4 ± 2.6	0.91 ± 0.44
	$u_{\phi,0}$ (μs)	1546.5 ± 7.8	

the velocity, we must take only the vertical component of lift generated by the rotors, i.e., we must replace u with $u_\phi = u\cos\phi$, where ϕ is the tilt angle and calculated as $\phi = \arctan\left(\sqrt{\tan^2\theta + \tan^2\nu}\right)$

Following the flight dynamics model used by AirSim [33], the solution to steady state (where the net force vanishes) in vertical flight is

$$< V_{\mathrm{U}}^{\mathrm{Air}} >^2 = sign\left(< V_{\mathrm{U}}^{\mathrm{Air}} >\right)\left(a' < u_\phi > -b'\right) \tag{1}$$

with

$$a' = \frac{8C_{\mathrm{T}}\omega_{\max}^2 D^4}{SC_{\mathrm{lin}}u_{\max}}; \quad b' = \frac{2mg}{\rho SC_{\mathrm{lin}}}$$

where W_{Z} is the vertical speed of the air, $< V_{\mathrm{U}}^{\mathrm{Air}} >=< V_{\mathrm{U}} > - W_{\mathrm{Z}}$ is the vertical velocity of the drone relative to the air, m and S are the mass and cross-section area of the vehicle, respectively, D and $\omega_{\max}$ are the diameter and maximum angular velocity, and C_{T} is the thrust coefficient of the propellers. $u_{\max}$ is the maximum pulse width of the speed controller Pulse Width Modulation. C_{lin} is the linear air drag coefficient. ρ is the air density and g is the gravitational acceleration. a' and b' were defined to provide a compact formula. Conversely,

$$< u_\phi > = a\ sign\left(< V_{\mathrm{U}}^{\mathrm{Air}} >\right)\left|< V_{\mathrm{U}}^{\mathrm{Air}} >\right|^2 + b \tag{2}$$

$$a = (a')^{-1} = \frac{SC_{\mathrm{lin}}u_{\max}}{8C_{\mathrm{T}}\omega_{\max}^2 D^4}; \quad b = \frac{b'}{a'} = \frac{u_{\max}mg}{4C_{\mathrm{T}}\rho\omega_{\max}^2 D^4}$$

where a and b correspond to the free parameters to be used in the fit that follows. We have established the relation between these quantities and the air velocities by fitting a “signed quadratic” function

$$f(x) = x^3/|x| = x^2 sign(x) \tag{3}$$

with the following form:

$$< u_\phi > = A \cdot f\left(< V_{\mathrm{U}} > -W_{\mathrm{Z}}\right) + u_{\phi,0}, \tag{4}$$

where A and $u_{\phi,0}$ are the parameters for the fit.

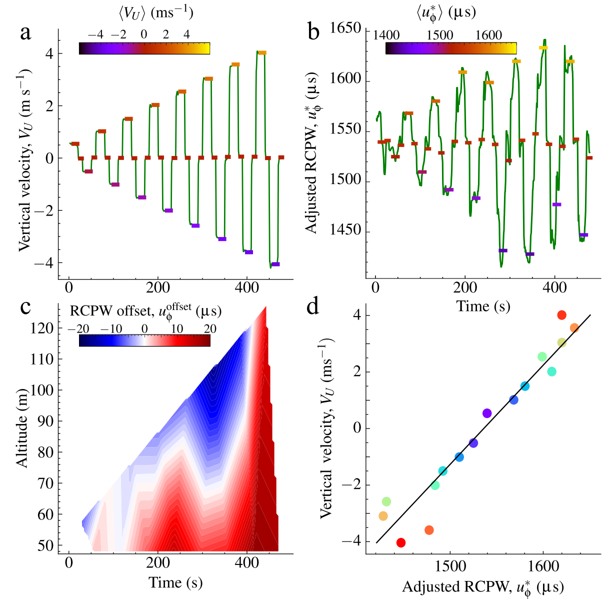

Fig. 3. **Example of the calibration protocol for a single drone. (a)** The dashed green line represents the vertical speed of the drone. **(b)** Adjusted pulse width of the speed controller (RCPW), the indicator of the rotor rotation speed with adjustment made based on the tilt angle ϕ. Colored line segments in panels (a) and (b) depict the window averages, with their lengths indicating the time period used for calculation and their color corresponding to the values in the colorbar. **(c)** The estimated offset, subtracted from the RCPW, is presented as a function of time (x-axis) and altitude (y-axis). The color gradient encodes the offset value, ranging from negative (blue) through zero (white) to positive (red). **(d)** Mapping of the vertical velocity (V_{U}) as a function of the RCPW. Circles represent the scatter plot of the mean values of RCPW and V_{U} taken within each window, as illustrated in panels (a) and (b). The color of each circle indicates the temporal progression of the measurement, from the first (purple) to the last (red). The solid black line represents the linear function that best fits the data.

C. Multidrone Field Experiment

A fleet of 49 identical quadcopter “show” mini-drones were placed in a square grid configuration on an open field exposed to atmospheric air movements. In the air, each drone was 7 meters away from its closest neighbor. The quadcopters used were the Pixel show drones from Light Dynamix Ltd. [32], featuring a diagonal wheelbase of 233 mm and total takeoff weight of 400 g, with an F9-P dual-band Real-Time Kinematics (RTK) Global Navigation Satellite System (GNSS) receiver, receiving RTK corrections from a base station through the Skybrush system. The autopilot firmware was ArduCopter 4.4 (identical to the one used in the SITL simulations).

1) Calibration: The calibration flight protocol matched exactly the one used during the simulations. After take-off, all drones reached the baseline altitude of 20 m above ground level. All drones performed the protocol in synchrony, keeping the square grid formation mentioned above. During the calibration phase, 42 calibration flight logs were successfully retrieved (the rest could not be downloaded for unknown reasons).

2) Analysis: Since this calibration was run in the field, there was no guarantee that the vertical velocity of the air would be zero throughout the experiment. Using all the

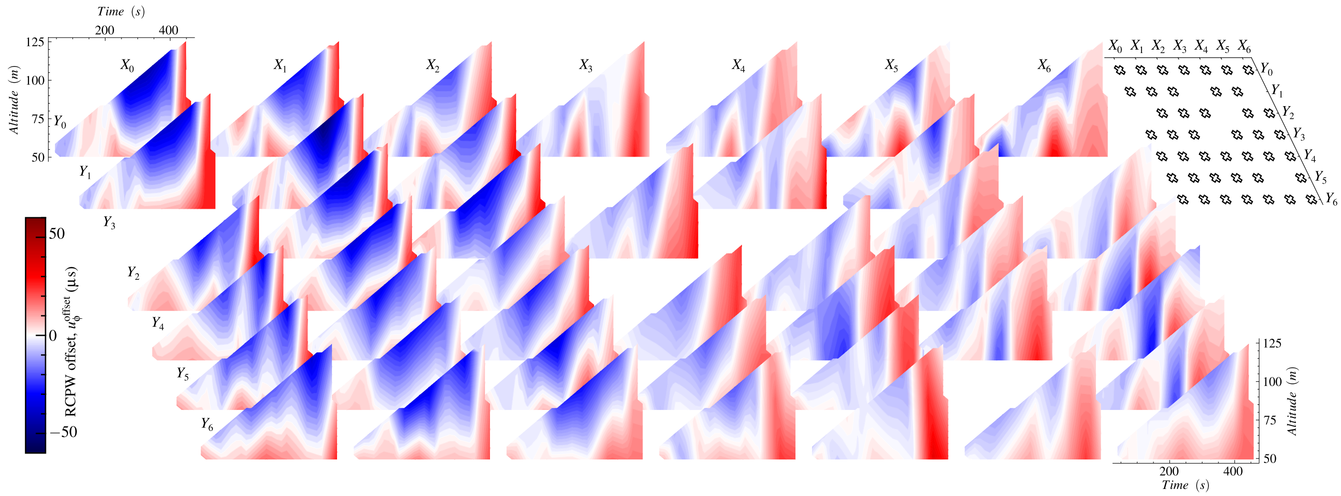

Fig. 4. **Estimated RCPW offset for the entire fleet**. The heatmaps illustrate the dependency of the u_ϕ^{offset} (color-encoded) as a function of time (x-axis) and altitude (y-axis) for each drone. The relative positions of the plots show the square grid configuration of the fleet during the calibration phase, as further illustrated in the top right corner. All plots share the same x-axis, y-axis and color encoding. Empty slots indicate that the flight log is not available.

windows corresponding to a desired velocity of $v_z^{\text{Desired}} = 0\ ms^{-1}$, – denoted as "0-window" – we have established the baseline RCPW under the assumption that a long enough average of vertical velocity of the air vanishes:

$$u_\phi^{\text{baseline}} = < u_\phi(t) >_{v_z^{\text{Desired}}=0} \tag{5}$$

Consequently, deviations from u_ϕ^{baseline} in individual 0-window imply local air movements. The method described already works if the calibration occurs in still air. To extend beyond that, we introduce a correction term, $u_\phi^{\text{offset}} = u_\phi - u_\phi^{\text{baseline}}$, to compensate the local air movements during the calibration procedure. Taking the average of the altitude, h, the time, t, and u_ϕ^{offset} in each 0-window, and using a linear interpolator, we establish a relation $u_\phi^{\text{offset}}(t, h)$, which we use to find the local offset for all points. Finally we define the adjusted RCPW as $u_\phi^* = u_\phi - u_\phi^{\text{offset}}$. To accommodate difference between the drones (such as battery performance or manufacturing imperfections/tolerance), this procedure was performed individually for each drone, i.e., each drone in the fleet had its own interpolator, which was determined with its own u_ϕ^{baseline} and averages of altitude and time (Fig. 4). The adjusted RCPW is then the quantity utilized in the fit to find the mapping between RCPW and V_{U}, as explained in Section II-B.2.

An additional mapping – denoted "flock mapping" – was determined by performing a fit with the averages of all the drones present in the calibration flight. Fig. 3 shows the entire calibration process for a single drone.

3) Measurement: Flying in the same horizontal grid formation, the same fleet was set to hover ($\vec{v}^{\text{Desired}} = \vec{0}\ ms^{-1}$) at an altitude of $100m$ above the ground for 10 minutes. In this phase of the experiment, 43 hovering flight logs could be retrieved successfully.

With a running window of 10 seconds (same as in the calibration), the average and standard deviation of V_{U}, u_ϕ, time, latitude and longitude were calculated individually for each drone, denoted by $< \cdot >_{10}$. Using $< u_\phi >_{10}$, we then applied each drone's mapping function to calculate the vertical velocity relative to air, V_U^{Air}, (i.e., the vertical velocity in still air), which we could use to calculate the vertical velocity of the air relative to the ground as a function of time:

$$< V_U^{\text{Air}} >_{10}(t) = f\left(< u_\phi >_{10}(t)\right) \tag{6}$$

$$< W_Z^* >_{10}(t) = < V_{\text{U}} >_{10}(t) - f\left(< u_\phi >_{10}(t)\right) \tag{7}$$

In the cases where a drone did not have a mapping determined in the calibration phase, the "flock mapping" was used instead.

Since logging is not synchronized between drones, to ensure synchrony in the updraft data, the time series of each drone was resampled by taking the average of the estimated updraft in each non-overlapping (synchronized) 1-second interval.

To further study the structure of the updraft speed, correlation functions were calculated in space and time as follows:

$$C\left(\Delta r_{i,j}\right) = < \hat{u}\left(t, \mathbf{r}_i\right) \hat{u}\left(t, \mathbf{r}_i + \Delta \mathbf{r}_{i,j}\right) >_t \tag{8}$$

$$C\left(\Delta t, \mathbf{r}_i\right) = < \hat{u}\left(t, \mathbf{r}_i\right) \hat{u}\left(t + \Delta t, \mathbf{r}_i\right) > \tag{9}$$

where $\mathbf{r}_i$ represents the positions of i-th drone and $\Delta r_{i,j} = |\Delta \mathbf{r}_{i,j}| = |\mathbf{r}_j - \mathbf{r}_i|$ is the relative distance between the i-th and the j-th drone.

The spatial correlation between pairs of drones in the subsamples of constant nominal distance was aggregated. The functional form of spatial correlation was asserted by using an exponential function, $f(x) = e^{-x/\lambda}$, to fit the median correlation in each subsample as a function of the median distance.

III. Results

A. Simulation

Equation 4 was used on an initial fit performed against the results of simulations in which the updraft was absent.

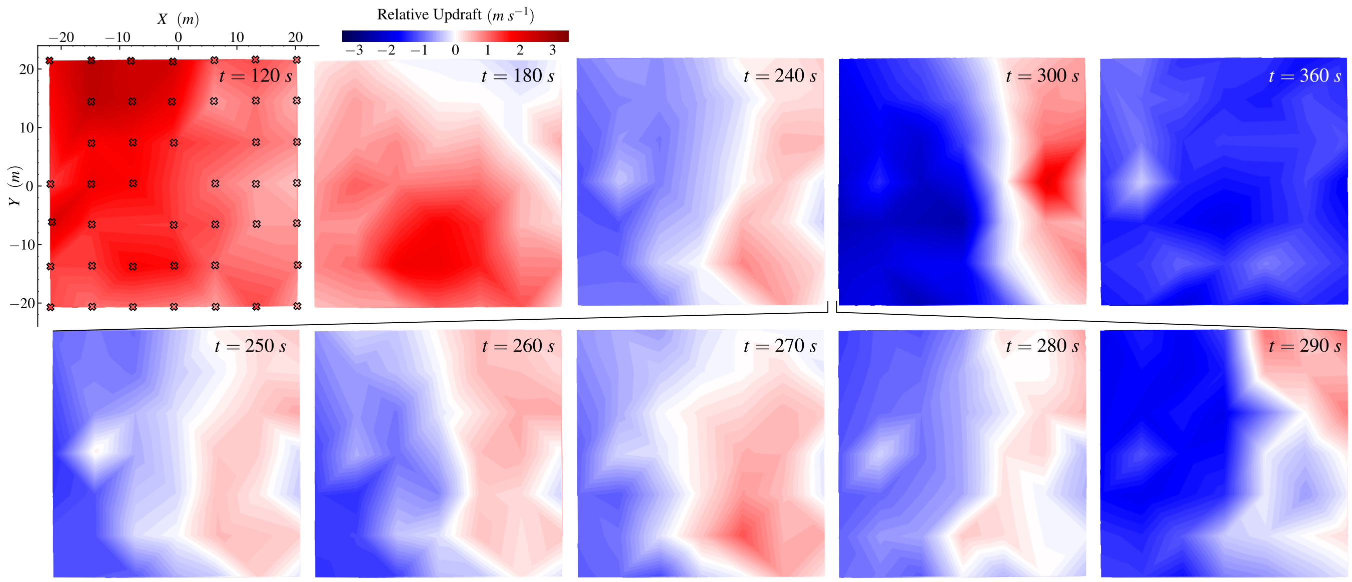

Fig. 5. Time evolution of the estimated vertical velocity profile of the air illustrated at different moments, as indicated in the top right corner of each panel. The top left panel additionally shows the positions of the drones, represented by crosses. The heatmaps display the color-encoded linear interpolation of the estimated vertical velocity of the air at each drone's location, with blue indicating air moving downwards and red representing upwards movement. All heatmaps share the same set of axes and color encoding. The top row presents heatmaps separated by 60 seconds, while the bottom row offers a more detailed view of the evolution of the velocity field over time, separated by 10 seconds.

The optimal parameters are presented in Table I. The fits to the results of the remaining simulations were performed keeping the values of A and $u_{\phi,0}$ fixed, leaving W_{Z} as the parameter to fit. See Fig. 2 for an example of the fits in windless conditions. The results show that in the simulation data, this method can reliably predict the present updraft, yielding Pearson's correlations $\rho \in [0.9996, 0.99999], n = 11, p \in [10^{-26}, 10^{-11}]$). Since our model does not depend on either the roll or the pitch angles, these statistics attest to the robustness of the method.

B. Field Experiments

1) Calibration: Equation (4) was used to find the mapping between RCPW and $V_{\mathrm{U}}^{\mathrm{Air}}$. However, despite being supported by theory and the simulation work, the resulting fits to the experimental data of many drones did not yield satisfactory results. In Table II, the best parameter values are shown, where one can see the large standard deviation of W_{Z} – the desired output of this project – and the large deviation from data in χ^2_ν. For this reason, a linear approximation ($f^*(x) = A'x + f_0^*$) was applied here to fit the experimental data, showing a much better agreement between its predicted values and the observed values. See Table II and Fig. 3d.

2) Measurement: The running averages of the 10-second windows were calculated and were passed to each drone's optimal fit of linear function, f^*. From this, we calculated the vertical velocity of the drone relative to the air and finally the vertical velocity of the air relative to the ground. Since these calculations were performed individually for each drone, what was achieved is, in fact, an estimated vertical velocity of the air as a function of time and space. Finally, the updraft was resampled into synchronized 1-second intervals. Fig. 5 shows the spatial distribution of the estimated updraft at different points in time, depicting a relatively smooth time evolution between the completely independent measurements[1].

Equations (8) and (9) were used to calculate the spatial and temporal correlations functions of the updraft velocity (Fig. 6a and 6b). By fitting an exponential function, the characteristic length was found to be $\lambda = 145.4 \pm 3.0\ m$, which is approximately 20 times the distance between neighboring drones. To estimate the characteristic time scale, a linear function, $f(\Delta t) = A(\Delta t - t_0)$, was fitted to the points of positive correlation. The crossing of this line with the horizontal axis was taken as the estimated time scale and was found to be $t_0 = 186.00 \pm 0.37\ s$. The anisotropy of the spatial correlation was also studied by taking the correlation between pairs of drones in the same row (Fig. 6c) or the same column (Fig. 6d). The characteristic lengths were found to be $\lambda_x = 121.3 \pm 6.8\ m$ and $\lambda_y = 252 \pm 18\ m$, respectively.

IV. Discussion

We presented a novel method for measuring the velocity profile of atmospheric convective updrafts using a fleet of affordable multirotor mini-drones. This approach included a comprehensive set of Software-in-the-Loop simulations, during which a drone flew in specific states in order to devise and assess the relationship between flight states and updraft speed. This mapping was achieved using only windless simulation flight logs and was evaluated through function fitting to all simulated flight logs, including those collected in windy conditions. The very high accuracy and precision of this method demonstrate strong robustness against varying wind

[1]For a more detailed visualization of this updraft field, please refer to the video in the following link: https://youtu.be/H7tvBqT5z4Y

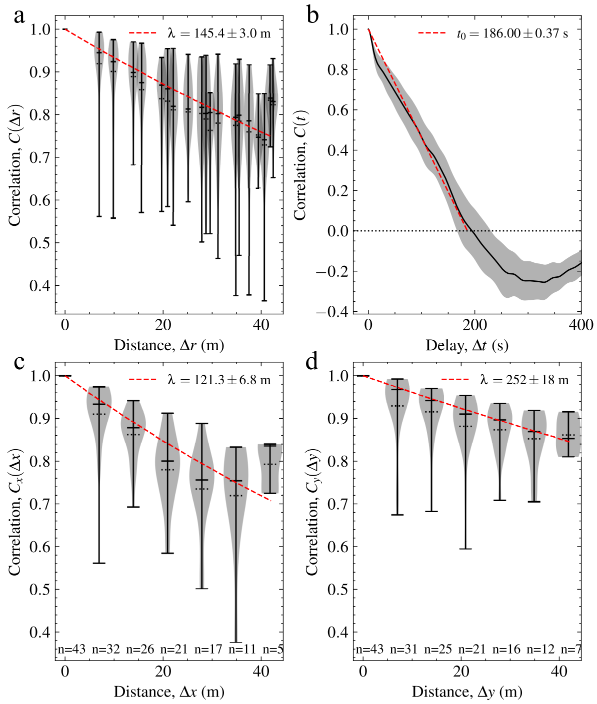

Fig. 6. **Spatial and temporal correlations present in the estimated vertical velocity of the air**. **(a)** Correlation between time series of the updraft speeds estimated by every possible pair of drones as a function of their relative distance. The violin plots aggregate the correlation attained from all pairs of drones with constant nominal distance (i.e., distance in the design square grid). In each violin plot, solid lines at the top and bottom show the extreme values, the solid line in the interior shows the median, and the dotted line indicates the sample mean. The red dashed line shows the best fit of the function $C^*(\Delta r) = e^{-\Delta r/\lambda}$ and optimal value of λ is presented on the legend. **(b)** Autocorrelation functions for the updraft's vertical speed time series as estimated by all drones, where the solid black line represents the mean, μ, of the sample and the gray shaded area shows the 1σ-deviation from the mean. The red dashed line shows the result of the fit of a linear function, $A\,(t - t_0)$, to the portion of the correlation function up to the first crossing with the horizontal axis. The optimal value for t_0 is shown on the legend. **(c)** and **(d)** show the spatial correlation of the updraft time series (similarly to panel (a)) separately along the 2 main axis of the grid created by the drones. Note that wind may considerably affect the characteristic length.

conditions. Subsequently, this procedure was shown to be effective in field experiments with multirotor drones, despite the additional complexities presented by real atmospheric flows, such as wind gusts and turbulence. While analyzing the data, we observed a considerable simulation-to-reality gap, and the data analysis pipeline required customization to effectively address the results of the field experiments. We note here that wind had very little, if any, effect on the procedure in the simulations; however, this shall be verified in field experiments, where external measurements of the wind need to be performed, preferably under diverse conditions. Moreover, these future experiments could be used to validate our assumptions, for example, to assess how long an average should be taken to define the baseline RCPW. However, if the measurement is performed immediately after the calibration (as in the case reported here), one could assume that the wind does not change significantly and, as such, its effect is accounted for in the calibration mapping, as part of the calculated tilt angle.

The flight logs of 43 independent measurements of individual drones showed high similarity between nearby measurements, allowing us to calculate temporal and spatial characteristics of air movement dynamics. The resulting updraft estimates describe smooth and consistent spatial fluctuations, which strengthens the validity of our findings.

The proposed framework relies on drones flying within the updraft, and by doing so, they affect the flow within the thermal. We aimed to minimize this effect by selecting small and lightweight drones with a relatively large distance between them. We also used relatively sparse spatial resolution as we wanted to cover areas as large as possible with the 49 drones that were available for this test measurement. However, considering the current industry standards, the number of minidrones (weighting typically less than 0.5kg) in such a system could easily be scaled up to include even thousands of units with centimeter-level positioning accuracy (similarly to the largest drone shows nowadays), allowing for a reduction in spacing while covering even larger areas (or even volumes) and creating highly detailed "tomographs" of the updraft. Alternatively, future experiments could include drones performing dynamic measurements with continuous motion to scan the air with an increased spatial resolution, by sacrificing temporal resolution.

Unlike the method proposed by [27], our approach employs multirotor drones, which offer several advantages over fixed-wing drones. Namely, the ability to hover in place without the need for a minimum velocity. This capability allows persistent point measurements in small areas or in locations that are challenging to reach. Furthermore, it could be used not only to measure but also to monitor severe weather events, as pointed out in [34]. The fleet proposed here could be used to study convective updrafts in detail, similarly to what was achieved for the vertical profile of horizontal wind [35]–[37].

In summary, the unique controllability, maneuverability, compact size, and large-scale availability of show minidrones offers an exciting opportunity for researchers to gain unprecedented insights into the dynamics of the air in general and of convective updrafts, in particular. These measurements also pave the way for the development of future autonomous, energy-efficient UAV control mechanisms along the entire path from data-driven realistic simulations to reality.

The potential impact of this research extends beyond thermal profiling and its use in innovative applications. The modality shift from drone shows to meteorological measurements is similar to the story of GPUs that were first required by the gaming industry but now provide the basics of many scientific calculations. Similarly, these off-the-shelf, commercially available drones are not even customized for meteorological studies, but their inherently accurate state estimation and detailed logging capabilities allow for the direct and indirect measurement of a wide variety of environmental variables, such as temperature, pressure, horizontal and vertical wind, etc. In addition, the simple scaling of show drone fleet size offers unprecedented volumetric, spatio-temporal mapping possibility of these variables with the mini drones as a standalone three-dimensional sensor array. In our data-driven world, these measurements can deepen the scientific understanding of meteorology and can also facilitate weather and climate predictions and model development.

ACKNOWLEDGMENT

Sources of funding include the Ministry of Culture and Innovation of Hungary from the National Research, Development and Innovation Fund (awarded to P.L., Project no. C1794246, KDP-2021 funding scheme), the Hungarian Academy of Sciences (grant number 95152, awarded to M.N.), Eötvös Loránd University, and CollMot Robotics Ltd. Large-scale field experiments were carried out by Light Dynamix Ltd. using Pixel drones and Skybrush software.

REFERENCES

[1] R. B. Stull, “Mean boundary layer characteristics,” in An introduction to boundary layer meteorology, Springer, 1988, pp. 1–27.

[2] S. C. Sherwood, S. Bony, and J.-L. Dufresne, “Spread in model climate sensitivity traced to atmospheric convective mixing,” Nature, vol. 505, no. 7481, pp. 37–42, Jan. 2014, doi: 10.1038/nature12829.

[3] S. C. Sullivan, D. Lee, L. Oreopoulos, and A. Nenes, “Role of updraft velocity in temporal variability of global cloud hydrometeor number,” Proceedings of the National Academy of Sciences, vol. 113, no. 21, pp. 5791–5796, 2016.

[4] A. Flack, M. Nagy, W. Fiedler, I. D. Couzin, and M. Wikelski, “From local collective behavior to global migratory patterns in white storks,” Science, vol. 360, no. 6391, pp. 911–914, 2018, doi: 10.1126/science.aap7781.

[5] R. Harel, N. Horvitz, and R. Nathan, “Adult vultures outperform juveniles in challenging thermal soaring conditions,” Scientific Reports, vol. 6, p. 27865, Jun. 2016, doi: 10.1038/srep27865.

[6] G. K. Taylor, K. V. Reynolds, and A. L. Thomas, “Soaring energetics and glide performance in a moving atmosphere,” Philosophical Transactions of the Royal Society B: Biological Sciences, vol. 371, no. 1704, p. 20150398, 2016.

[7] H. J. Williams, A. J. King, O. Duriez, L. Börger, and E. L. Shepard, “Social eavesdropping allows for a more risky gliding strategy by thermal-soaring birds,” Journal of the Royal Society Interface, vol. 15, no. 148, p. 20180578, 2018.

[8] Z. Ákos, M. Nagy, and Tamás Vicsek, “Comparing bird and human soaring strategies,” Proceedings of the National Academy of Sciences, vol. 105, no. 11, pp. 4139–4143, 2008, doi: 10.1073/pnas.0707711105.

[9] M. Allen, “Autonomous Soaring for Improved Endurance of a Small Uninhabitated Air Vehicle,” in 43rd AIAA Aerospace Sciences Meeting and Exhibit, AIAA, 2005. doi: 10.2514/6.2005-1025.

[10] Z. Akos, M. Nagy, S. Leven, and T. Vicsek, “Thermal soaring flight of birds and unmanned aerial vehicles,” Bioinspiration & biomimetics, vol. 5, no. 4, p. 045003, 2010.

[11] J. Wharington and R. M. I. of Technology (Australia), Autonomous Control of Soaring Aircraft by Reinforcement Learning. Royal Melbourne Institute of Technology, 1998.

[12] M. Allen and V. Lin, “Guidance and Control of an Autonomous Soaring Vehicle with Flight Test Results,” in 45th AIAA Aerospace Sciences Meeting and Exhibit, AIAA, 2007. doi: 10.2514/6.2007-867.

[13] D. J. Edwards and L. M. Silverberg, “Autonomous Soaring: The Montague Cross-Country Challenge,” Journal of Aircraft, vol. 47, no. 5, pp. 1763–1769, 2010, doi: 10.2514/1.C000287.

[14] G. Reddy, A. Celani, T. J. Sejnowski, and M. Vergassola, “Learning to soar in turbulent environments,” Proceedings of the National Academy of Sciences, vol. 113, no. 33, pp. E4877–E4884, Aug. 2016, doi: 10.1073/pnas.1606075113.

[15] G. Reddy, J. Wong-Ng, A. Celani, T. J. Sejnowski, and M. Vergassola, “Glider soaring via reinforcement learning in the field,” Nature, vol. 562, pp. 236–239, Oct. 2018, doi: 10.1038/s41586-018-0533-0.

[16] D. Edwards, “Implementation Details and Flight Test Results of an Autonomous Soaring Controller,” in AIAA Guidance, Navigation and Control Conference and Exhibit, AIAA, 2008. doi: 10.2514/6.2008-7244.

[17] M. J. Allen, “Updraft model for development of autonomous soaring uninhabited air vehicles,” Collection of Technical Papers - 44th AIAA Aerospace Sciences Meeting, vol. 24, pp. 18028–18046, 2006, doi: 10.2514/6.2006-1510.

[18] D. H. Lenschow and P. L. Stephens, “The role of thermals in the convective boundary layer,” Boundary-Layer Meteorology, vol. 19, no. 4, pp. 509–532, 1980, doi: 10.1007/BF00122351.

[19] G. S. Young, “Turbulence Structure of the Convective Boundary Layer. Part I. Variability of Normalized Turbulence Statistics,” Journal of the Atmospheric Sciences, vol. 45, no. 4, pp. 719–726, Feb. 1988, doi: 10.1175/1520-0469(1988)045¡0719:TSOTCB¿2.0.CO;2.

[20] G. S. Young, “Turbulence structure of the convective boundary layer. Part II: Phoenix 78 aircraft observations of thermals and their environment,” Journal of the Atmospheric Sciences, vol. 45, no. 4, pp. 727–735, 1988, doi: 10.1175/1520-0469(1988)045¡0727:TSOTCB¡2.0.CO;2.

[21] I. de Boisblanc et al., “Designing a hexacopter for the collection of atmospheric flow data,” in 2014 Systems and Information Engineering Design Symposium (SIEDS), IEEE, 2014, p. 25. doi: 10.1109/SIEDS.2014.6829915.

[22] C.-C. Chang, C.-Y. Chang, J.-L. Wang, X.-X. Pan, Y.-C. Chen, and Y.-J. Ho, “An optimized multicopter UAV sounding technique (MUST) for probing comprehensive atmospheric variables,” Chemosphere, vol. 254, p. 126867, Sep. 2020, doi: 10.1016/j.chemosphere.2020.126867.

[23] R. T. Palomaki, N. T. Rose, M. van den Bossche, T. J. Sherman, and S. F. J. De Wekker, “Wind Estimation in the Lower Atmosphere Using Multirotor Aircraft,” Journal of Atmospheric and Oceanic Technology, vol. 34, no. 5, pp. 1183–1191, May 2017, doi: 10.1175/JTECH-D-16-0177.1.

[24] G. W. Donnell, J. A. Feight, N. Lannan, and J. D. Jacob, “Wind Characterization Using Onboard IMU of sUAS,” in 2018 Atmospheric Flight Mechanics Conference, AIAA, 2018. doi: 10.2514/6.2018-2986.

[25] C. Brosy et al., “Simultaneous multicopter-based air sampling and sensing of meteorological variables,” Atmospheric Measurement Techniques, vol. 10, no. 8, pp. 2773–2784, 2017, doi: 10.5194/amt-10-2773-2017.

[26] P. Abichandani, D. Lobo, G. Ford, D. Bucci, and M. Kam, “Wind Measurement and Simulation Techniques in Multi-Rotor Small Unmanned Aerial Vehicles,” IEEE Access, vol. 8, pp. 54910–54927, 2020, doi: 10.1109/ACCESS.2020.2977693.

[27] P. Tian and H. Chao, “Model Aided Estimation of Angle of Attack, Sideslip Angle, and 3D Wind without Flow Angle Measurements,” in 2018 AIAA Guidance, Navigation, and Control Conference, AIAA, 2018. doi: 10.2514/6.2018-1844.

[28] K. Meier, R. Hann, J. Skaloud, and A. Garreau, “Wind Estimation with Multirotor UAVs,” Atmosphere, vol. 13, no. 4, 2022, doi: 10.3390/atmos13040551.

[29] C. R. Ltd., “Skybrush drone swarm control software suite.” https://skybrush.io

[30] M. Research, “Microsoft AirSim.” https://microsoft.github.io/AirSim/

[31] C. R. Ltd., “ArduCopter forked by Skybrush.” https://github.com/skybrush-io/ardupilot/tree/CMCopter-4.4

[32] L. D. Ltd., “Pixel show drones.” https://www.lightdynamix.co.uk/pixel

[33] S. Shah, D. Dey, C. Lovett, and A. Kapoor, “AirSim: High-Fidelity Visual and Physical Simulation for Autonomous Vehicles,” 2017. [Online]. Available: https://arxiv.org/abs/1705.05065

[34] E. W. Frew, J. Elston, B. Argrow, A. Houston, and E. Rasmussen, “Sampling Severe Local Storms and Related Phenomena: Using Unmanned Aircraft Systems,” IEEE Robotics & Automation Magazine, vol. 19, no. 1, pp. 85–95, Feb. 2012, doi: 10.1109/MRA.2012.2184193.

[35] T. Wetz, N. Wildmann, and F. Beyrich, “Distributed wind measurements with multiple quadrotor unmanned aerial vehicles in the atmospheric boundary layer,” Atmospheric Measurement Techniques, vol. 14, no. 5, pp. 3795–3814, May 2021, doi: 10.5194/amt-14-3795-2021.

[36] H. Chen, H. Bai, and C. N. Taylor, “Wind Field Estimation Using Multiple Quadcopters,” IFAC-PapersOnLine, vol. 56, no. 3, pp. 61–66, Jan. 2023, doi: 10.1016/j.ifacol.2023.12.001.

[37] H. Chao and Y. Chen, “Surface wind profile measurement using multiple small unmanned aerial vehicles,” in Proceedings of the 2010 American Control Conference, 2010, pp. 4133–4138. doi: 10.1109/ACC.2010.5530609.